Integration of GNSS and LEO-PNT for Precise Positioning: a Simulation in Urban Environment

Marianna Alghisi[1,*,†], Ludovico Biagi[1]

[1]Politecnico di Milano, Milano, Italy

Abstract

The demand for accurate, real-time positioning is increasing across various domains, including autonomous navigation, public safety, urban mobility, and assistive technologies. While Global Navigation Satellite Systems (GNSS) provide global coverage and reliable Positioning, Navigation, and Timing (PNT) services, their performance in dense urban environments remains a challenge due to signal obstructions, multipath effects, and interference threats such as spoofing and jamming. To enhance positioning performance in such scenarios, this study explores the integration of Low Earth Orbit (LEO)-based PNT constellations with GNSS, focusing on their impact on Precise Point Positioning (PPP) convergence time. A simulated LEO-PNT constellation of 263 satellites, operating at 1200 km altitude with polar or 55° inclined orbits, is introduced to augment GNSS observables. Using real GNSS data and an Extended Kalman Filter (EKF) approach, the hybrid GNSS+LEO system is evaluated in a simulated urban environment with a 40° elevation cutoff. The results, based on three test datasets, demonstrate a significant reduction in PPP convergence time, up to 80% improvement in challenging conditions, highlighting the potential of LEO-PNT in enabling faster and more reliable positioning solutions for future urban applications.

Keywords

GNSS, LEO-PNT, Precise Point Positioning, Urban Environment

1. Introduction

Nowadays, positioning and navigation of people and vehicles is a need for society: the computation of precise position, in real time and single epoch, is fundamental for many applications, such as guidance and control, industrial applications, mass market, public security, assistive technologies and recreational purposes. Precise positioning plays a central role in the distribution of the future cities' services and applications. For instance autonomous driving relies on GNSS (Global Navigation Satellite System), sensors, radar and advanced positioning techniques to enable vehicles to operate without human intervention. In addition, the knowledge of accurate vehicle positioning facilitates traffic optimization, particularly by improving road safety, enhancing the reduction of emissions and contributing to more sustainable urban mobility. Furthermore, location-based services provide personalized information and services based on the user's location, enabling real-time traffic updates, efficient public transportation, and shared mobility solutions such as bike or car-sharing and ride-hailing services. The optimization of urban mobility improve the overall efficiency of transportation systems. Another example are assistive services for people with disabilities. Innovations such as obstacle detection systems, location-based audio guides, and navigation tools improve accessibility, ensuring safer and more inclusive public spaces. At present, most positioning, navigation, and timing (PNT) services rely on the use of Global Navigation Satellite Systems (GNSS). With GNSS we intend all the constellations of satellites properly designed to provide PNT information to users on the ground, in MEO (Medium, Earth Orbith) and GEO (Geosynchronous Earth Orbit). These systems guarantee global coverage and are designed to operate reliably under all weather conditions, making them indispensable for a wide range of applications across various domains. The four primary systems are the Global Positioning System (GPS) from the United States, Galileo from Europe, the BeiDou Navigation Satellite System (BDS) from China, and the Global

WIPHAL'25: Work-in-Progress in Hardware and Software for Location Computation June 10–12, 2025, Rome, Italy

*Corresponding author.

†These authors contributed equally.

marianna.alghisi@polimi.it (M. Alghisi); ludovico.biagi@polimi.it (L. Biagi)

0000-0001-5439-0145 (M. Alghisi)

Navigation Satellite System (GLONASS) from Russia. Additionally, several regional satellite navigation systems have been developed, such as the Indian Regional Navigation Satellite System (IRNSS) in India and the Quasi-Zenith Satellite System (QZSS) in Japan [1], [2]. The standard point positioning in open field can be considered since several years a globally achieved goal: processing of multi-frequencies pseudoranges can provide accuracies at the meter level. Precise Point Positioning (PPP), [3] and network geodetic processing of phase observations push accuracies up to the cm / mm level, [4], [5], [6], [7]. On the contrary, positioning in densely inhabited and built urban environments still remains an open challenge, because the scenario affects the accuracy, the reliability and even the availability of PNT services: buildings, underpasses, moving vehicles, even vegetation block the signals from many satellites, causing a poor, or even not solvable geometry [8], [9], [10]. In addition to the challenges related to satellite availability, caused by the presence of physical obstructions, another significant factor limiting GNSS operability is the rise of spoofing and jamming incidents [11],[12],[13]. Therefore, in a modern scenario GNSS solutions could be significantly aided by the introduction of additional positioning observations, that improve both the geometric configuration and the system redundancy. In recent years, there have been several attempts to integrate various positioning technologies, with particular attention focused on the potential applications of 5G technology for positioning solutions [14], [15], [16]. There has been increasing discussion about LEO-PNT (Low Earth Orbit Positioning, Navigation, and Timing) thanks to institutional initiatives (e.g., ESA) and private companies (such as Centispace [17] and Xona Space [18]). LEO-PNT refers to a constellation of Low Earth Orbit (LEO) satellites specifically designed to provide Positioning, Navigation, and Timing (PNT) services. LEO satellites operate at altitudes ranging approximately between 400 km and 1,500 km, which distinguishes them by reducing free-space losses and atmospheric disturbances. This enables stronger signals, thereby enhancing reliability and performance in challenging environments [19], [20], [21]. The aim of this work is to assess how the introduction of a LEO-PNT system can enhance PPP performance in a simulated urban environment. Specifically, we seek to analyze how the inclusion of code-only signals from a LEO constellation can help reduce the convergence time of GNSS based PPP. By leveraging real GNSS data, algorithms and software have been developed to jointly process pseudorange and phase observables with and Extended Kalman Filter (EKF) to estimate UE (User Equipment) location. To assess potential improvements, we simulate the orbits of a LEO-PNT constellation along with the corresponding pseudorange observables. Specifically, we model a constellation of 263 satellites distributed in orbits with either polar inclination or a 55° inclination. The orbital dynamics are computed over a full 24-hour period. The pseudorange observables transmitted from each LEO satellite to a receiver at a known location are simulated according to the methodologies detailed in Section 2.3. The improvements obtainable from the joint processing of GNSS and LEO-PNT are evaluated comparing the convergence time required to target a 2D accuracy of 30 cm in a GNSS-only system with respect to the hybrid system in a simulated urban environment. In particular, the urban environment is simulated through the introduction of a cutoff on satellites' elevation of 40 degrees.

2. Positioning Models and Methods

This section outlines the positioning models and the corresponding observation equations for the measurements processed in the positioning software. Specifically, the software processes iono-free GNSS code and phase observables, as well as simulated iono-free LEO-PNT code observables. The system uses an EKF to process these measurements. Additionally, a detailed description of the EKF implementation is provided, outlining its role in improving the accuracy and convergence of the positioning solution.

2.1. GNSS Positioning Model

GNSS satellites, according to the literature, transmit observables modeled at different frequencies within the L-band. Therefore, with a multi-frequency receiver, it is possible to obtain multiple observations from the same satellite at a given epoch. These observations can be combined to generate several

new observables, among all of them we are going to focus on ionospheric-free observations, which are a combination of GNSS measurements that eliminates the effects of ionospheric delay, which can introduce errors in positioning solutions. According to standard literature [1], [2], the ionospheric free code observation equation P_{UE}^{IF} and phase observation equation Φ_{UE}^{IF} from satellite s tracked by receiver UE at epoch t, s belongs to GNSS constellation S, are reported in the following:

$$\begin{aligned} P_{UE}^{IF,s}(t) =& \rho_{UE}^{s}(t-\tau_{UE}^{s}) + T_{UE}^{s}(t) \\ &+ c(dt_{UE}(t) + d_{UE,P}^{S,IF}) + c \times dt^{s}(t-\tau_{UE}^{s}) + \nu(t) \end{aligned} \tag{1}$$

$$\begin{aligned} \Phi_{UE}^{IF,s}(t) =& \rho_{UE}^{s}(t-\tau_{UE}^{s}) + T_{UE}^{s}(t) + c(dt_{UE}(t) + d_{UE,\Phi}^{S,IF}) + \\ & c \times dt^{s}(t-\tau_{UE}^{s}) + \eta(t)_{UE}^{\Phi,s} + \nu(t) \end{aligned} \tag{2}$$

where:

- $\rho_{UE}^{s} = ||X^{s} - X_{UE}||$ is the distance of the user with respect to the satellite s.
- τ_{UE}^{s} is the travel time between the satellite s and the UE.
- T_{UE}^{s} is the tropospheric delay between the satellite s and the UE.
- dt_{UE} is the clock bias of the UE.
- $d_{UE}^{S,IF}$ is the receiver code hardware bias, different for each constellation.
- dt^{s} is the clock bias of satellite s that includes the relative hardware bias.
- ν is the measurement noise.
- $\eta_{UE}^{\Phi,s}$ is the phase ambiguity of each mesurement, specific of each satellite.

The adopted notation refers to standard literature [1].

2.2. LEO-PNT Positioning Model

As previously introduced, the design and implementation of LEO-PNT constellation is still ongoing and it must consider factors such as cost, coverage, and signal quality in the definition of the final specifications. Decisions are still being made regarding the types of signals that will be onboard these satellites and the frequency bands they will operate on [20]. At present, we assume that LEO-PNT, as in GNSS, will allow the user to perform two different types of ranging measurements: code and phase observations. To guarantee backward compatibility, we assume that part of the measurements will be transmitted on the same band as GNSS and will be available on multiple frequencies, in order to be able to compute ionospheric free observables. In this work we are going to process only LEO-PNT pseudorange measurements. The non-linear code observation equation, for a LEO constellation L of $l = 1, ..., n$ satellites, at time of observation t is:

$$\begin{aligned} P_{UE}^{IF,l}(t) =& \rho_{UE}^{l}(t-\tau_{UE}^{l}) + T_{UE}^{l}(t) \\ &+ c(dt_{UE}(t) + d_{UE,P}^{L,IF}) + c \times dt^{s}(t-\tau_{UE}^{l}) + \nu(t) \end{aligned} \tag{3}$$

The observation equation for the phase measurement in the LEO-PNT system is omitted, as it is not utilized within the scope of this study. However, its structure can be considered analogous to that of conventional GNSS systems.

2.3. LEO-PNT constellation and measurements simulation

The LEO-PNT constellation was simulated with 263 satellites at an height of 1200 km. The constellation of 263 satellites is divided between two orbital configurations: a portion is distributed across polar orbital planes with an inclination of 89°, ensuring global coverage including high-latitude regions, while the remaining satellites are placed in planes inclined at 55°, optimized for enhanced coverage over mid-latitude, densely populated areas. The orbit is assumed to be circular, with eccentricity equal to 0.

The constellation follows a Keplerian orbital model and the relative orbital parameters were sumulated in order to optimize the coverage, following a constellation model consistent with the existing ESA literature related to the LEO-PNT project, which considers system architectures tailored for PNT applications [22], [20]. For the observable simulation, reference is made to equation 3, adopting the following simplifications:

$$\begin{aligned} P_{UE}^{IF,l}(t) =& \rho_{UE}^{l}(t-\tau_{UE}^{l}) + T_{UE}^{l}(t) + c(dt_{UE}(t) + d_{UE}^{L,IF}) \\ &+ \varepsilon_{CLOCK} + \varepsilon_{LEO} + \varepsilon_{TROPO} \end{aligned} \tag{4}$$

The satellite clock offset is neglected, as is supposed to be modeled and transmitted by the ephemerides, as happen in GNSS.Regarding the receiver clock offsets, the code-based clock offset is pre-estimated using the same processing software, relying solely on GNSS observations. A moving median filter, with a window of 60 epochs, is then applied to smooth the pre-estimated values and reduce the impact of outliers. Finally, a Gaussian random noise term ε_{CLOCK} is added. The receiver clock offset is subsequently estimated within the system model, as detailed in Section 2.4. The corresponding error, σ^2_{CLOCK}, is modeled as a residual error following a Random Walk process with standard deviation of 12.5 cm. ε_{LEO} comprehend the three components (radial, along- and cross-track) error bias modeled by a Random Walk with a standard deviation of 7.5cm [23]. For what concern the modeling of the tropospheric delay we compute the Zenital wet T_{ZWD} and hydrostatic T_{ZHD} delay an epoch t and we model it with the respective wet and hydrostatic Mapping function (Mf_{ZWD}, Mf_{ZHD}), depending on the satellite l position.

$$T_{UE}^{l}(t) = T_{ZHD}(t)Mf_{ZHD}(t) + T_{ZWD}(t)Mf_{ZWD}(t) \tag{5}$$

The respective ε_{TROPO} error bias is modeled according to a Random Walk with 2.5 cm standard deviation.

2.4. Hybrid positioning model

For what concern the implemented solution algorithm, GNSS and LEO measurements are jointly processed with an EKF. The system state is structured as follow:

$$\underline{\boldsymbol{x}} = \begin{bmatrix} \underline{\boldsymbol{X}}_{ITRF} \\ \underline{\boldsymbol{dt}}_{UE}^{S,P} \\ T_{ZWD} \\ \underline{\boldsymbol{\Theta}}_{UE}^{S,\Phi} \end{bmatrix} \tag{6}$$

$\underline{\boldsymbol{X}}_{ITRF}$ is the position of the receiver in ITRF. $\underline{\boldsymbol{dt}}_{UE}^{S,P}$ is the vector containing the clock offsets of the receiver with respect to code measurements, comprehending the UE clock offset and the receiver code hardware bias, different for each constellation: $dt_{UE}^{S,P} = dt_{UE,P} + d_{UE}^{S,IF}$. The number of $\underline{\boldsymbol{dt}}_{UE}^{S,P}$ is equal to the number of available constellations (MEO and LEO). T_{ZWD} is the zenithal wet tropospheric delay. $\underline{\boldsymbol{\Theta}}_{UE}^{S,\Phi}$ is a vector containing the unknown relative to phase measurements: $\Theta_{UE}^{S,\Phi} = c \times (dt_{UE,\Phi}(t) + d_{UE}^{S,IF}) + \eta(t)_{UE}^{\Phi,s}$. It is important to emphasize that this approach was adopted because the software is designed for navigation rather than geodetic processing. By structuring the system in this way, the number of unknowns is minimized, thereby maximizing system redundancy. For the EKF implementation we refer to standard literature [24], the implemented dynamic model is:

$$\widehat{\underline{\boldsymbol{x}}}_t = \boldsymbol{T}\underline{\boldsymbol{x}}_{t-1} + \underline{\boldsymbol{\varepsilon}}_t \tag{7}$$

where $\boldsymbol{T}$ represents the design matrix of the dynamic model, which is $T = I$ under the assumption of a nearly static system. $\widehat{\underline{\boldsymbol{x}}}_t$ denotes the predicted state at epoch t based on the dynamic model, while $\underline{\boldsymbol{\varepsilon}}_t$ represents the model error. A covariance matrix, $\boldsymbol{C}_t^{\boldsymbol{\varepsilon}}$, is assigned to the model error to account for its uncertainty: the standard deviation of the coordinates X, Y, Z is $0m$; the code clock offset $dt_{UE}^{S,P}$ is $5m$; the residual wet Tropospheric delay is $0.01cm$ and $\Theta_{UE}^{S,\Phi}$ is $10m$.

3. Results

The following section summarizes the results obtained from processing 12 hours of data acquired over three different days in 2024: Test 1 (DOY: 278), Test 2 (DOY: 289), Test 3 (DOY: 308). GNSS data were collected at a 1 Hz sampling rate from the permanent station in Milan, which is part of the SPIN GNSS network. SPIN (Sistema di Posizionamento Integrato Nazionale) is a high-precision GNSS network that provides continuous positioning services for geodetic, scientific, and engineering applications. The network consists of 39 reference stations distributed in the north of Italy. Only measurements from GPS, Galileo and BeiDou constellations have been processed.
For what concerns the LEO data, they've been simulated according to the methods described in Section 2.3. In order to have a better understanding of the satellite availability, in particular of the simulated LEO constellation, the number of the satellites in LOS is computed for 24 hours of data. Figure 1 shows the number of available GNSS satellites in open-sky condition (cutoff 0) and urban environment (cutoff 40); Figure 2 report the number of LoS satellites for LEO constellation in the same scenarios. It is evident that, in both cases the number of satellites decreases significantly after applying the cutoff. However, this condition affects more significantly LEO constellation: in many epochs we have no satellites in LoS, while for GNSS the minimum number of LoS satellites never gets lower 4.
Two different processing configurations are tested: GNSS-only and hybrid GNSS+LEO. Since this work aims to assess the improvements in PPP convergence time in challenging environments such as urban canyons, a satellite elevation cutoff of 40 degrees is applied to satellite's measurements. The UE location is then estimated using the EKF and compared with the true position of the network base station (BS) as provided by SPIN. The errors in the East, North, and Up components are computed, along with the overall 2D error, for both tested configuration. To evaluate the improvement in convergence time, we identify the last epoch in the time series where the 2D error exceeds the 30 cm threshold. From that point onward, the error remains below this threshold, consistently meeting our accuracy requirement. Table 1 reports the convergence time (in minutes) for both GNSS-only and GNSS+LEO configurations for all the tested days. The results show a significant improvement in convergence time, reaching up to an 80% reduction on the day with the worst performance GNSS-only (DOY = 308). Figures 3, 4, 5

Table 1
Time required for the filter to converge to a 2D error smaller than 30 cm.

Date	Test	Configuration	Convergence time [min]
4/10/24	1	GNSS	9.8
4/10/24	1	GNSS+LEO	3.15
15/10/24	2	GNSS	20.3
15/10/24	2	GNSS+LEO	14.4
3/11/24	3	GNSS	31.7
3/11/24	3	GNSS+LEO	5.8

show the 2D error trend over time, focusing on the first hour for better visualization of the convergence process, as the solution remains stable once convergence is achieved. It is clearly visible that with the introduction of LEO, the increased number of satellites in LOS helps both to reduce the convergence time and to stabilize the solution more quickly over time. Tables 2 and 3 report the statistical analysis of the time series of the East, North, and Up errors once convergence is reached. It is evident that the solution is stable and optimal in both GNSS-only and GNSS+LEO configurations, with average errors at the centimeter level for both the components. However, the introduction of LEO helps reduce the standard deviation, bringing it to the millimeter level for the horizontal components. In conclusion, the introduction of LEO can significantly improve the convergence time of the PPP solution, making it more efficient and reliable. The analysis demonstrates that the increased number of satellites in line-of-sight (LOS) provided by LEO enhances both the speed of convergence and the overall stability of the solution. In addition, even if with the application of a 40-degree cutoff the number of LEO satellites

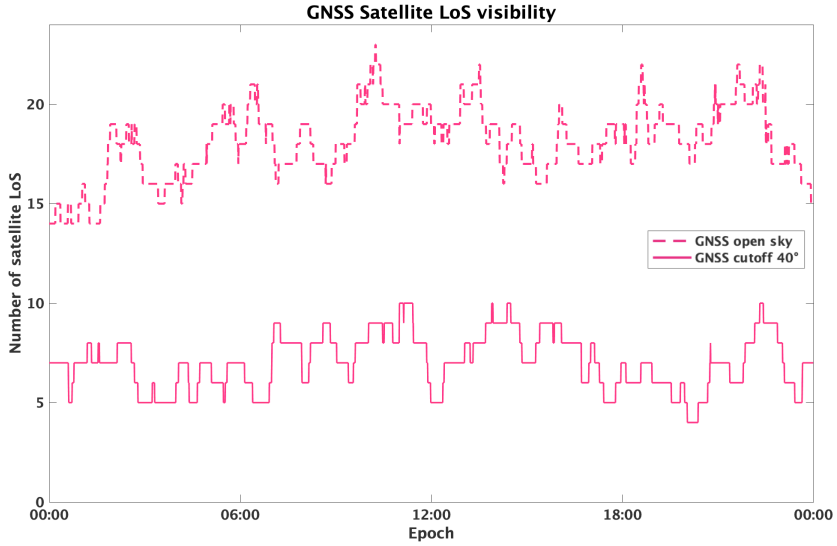

Figure 1: GNSS Satellite availability in open sky (0 cutoff applied) an urban environment (40 cutoff applied).

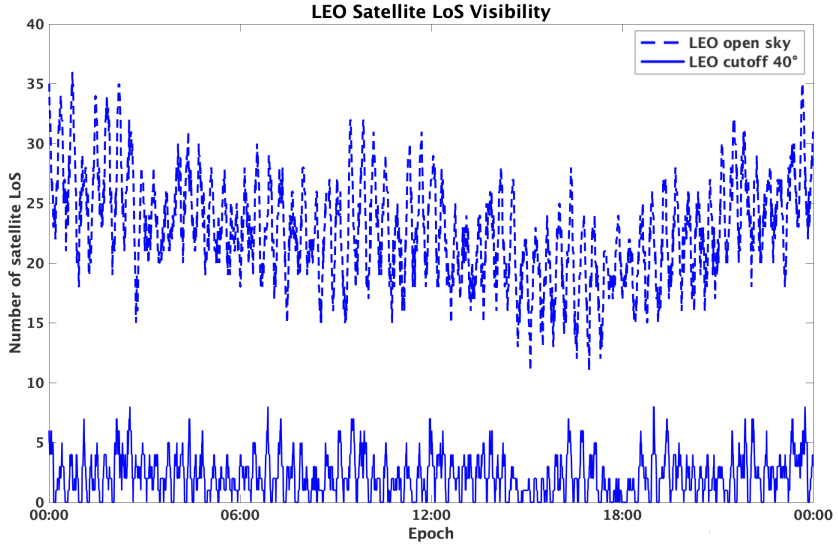

Figure 2: LEO Satellite availability in open sky (0 cutoff applied) an urban environment (40 cutoff applied).

Table 2
Statistical anlysis of GNSS-only results.

Test	**Mean[m]**			**STD** [m]		
	East	North	Up	East	North	Up
1	0.04	0.05	0.02	0.01	0.01	0.04
2	0.03	0.08	0.01	0.02	0.01	0.06
3	0.03	0.05	0.05	0.03	0.04	0.04

is very reduced and can reach zero for some epochs, LEO satellites still contribute significantly to reduce the convergence times. This is also due to their faster geometry and the fact that, traveling at nearly twice the speed of GNSS satellites, periods of signal outage are limited. Additionally, the statistical evaluation of positioning errors highlights a reduction in standard deviation, particularly for the horizontal components, reaching the millimeter level. These findings suggest that integrating LEO into GNSS can be a valuable enhancement for precise positioning applications, especially in challenging

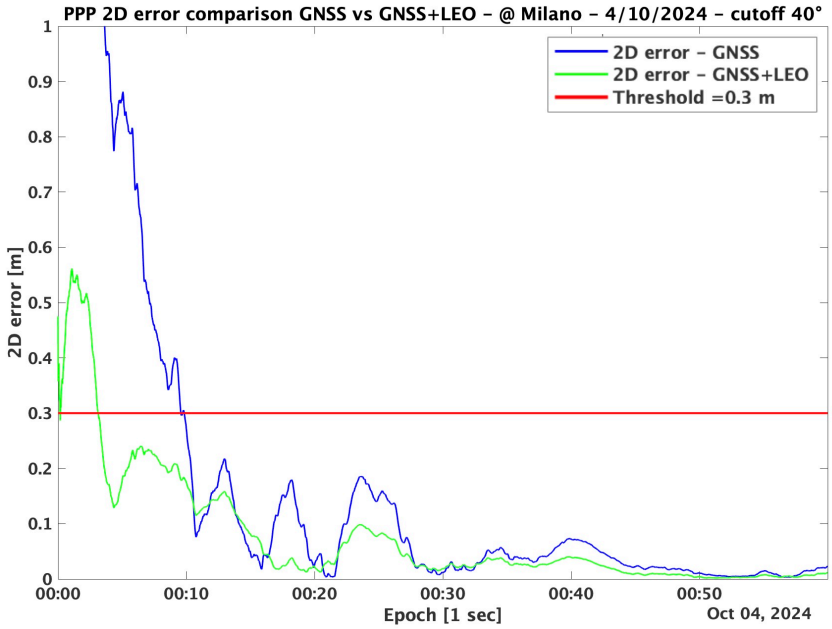

Figure 3: Comparison of 2D error over time for GNSS-only (bleue) configuration and hybrid GNSS+LEO (green) configuration for Test 1 (DOY: 278)

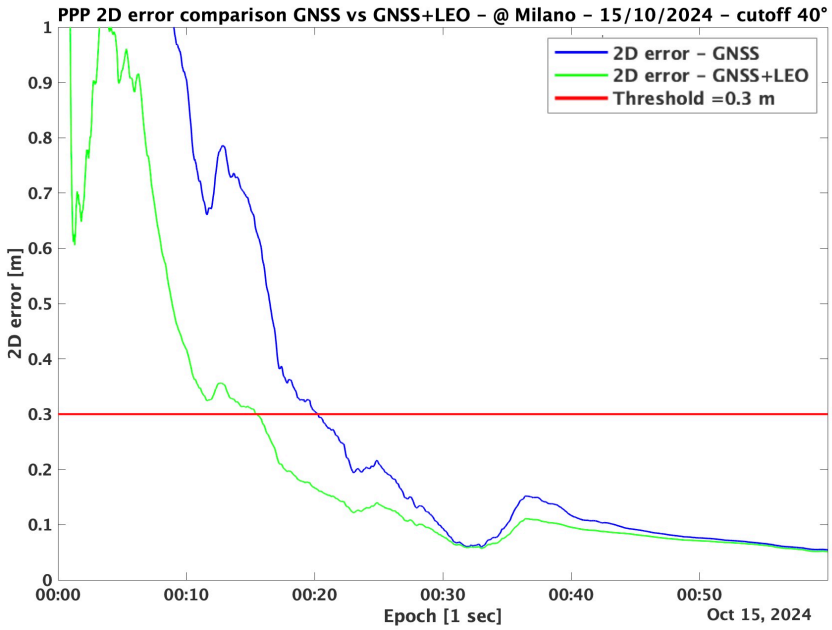

Figure 4: Comparison of 2D error over time for GNSS-only (blue) configuration and hybrid GNSS+LEO (green) configuration for Test 2 (DOY: 289)

environments where rapid convergence and high accuracy are crucial. The next steps of this work include conducting a measurement campaign using a GNSS receiver in an urban environment to collect real data in both static and kinematic conditions. This will enable testing of real scenarios with the developed software using field-collected measurements. These steps will provide further validation of the proposed approach and assess its performance in more challenging and dynamic conditions.

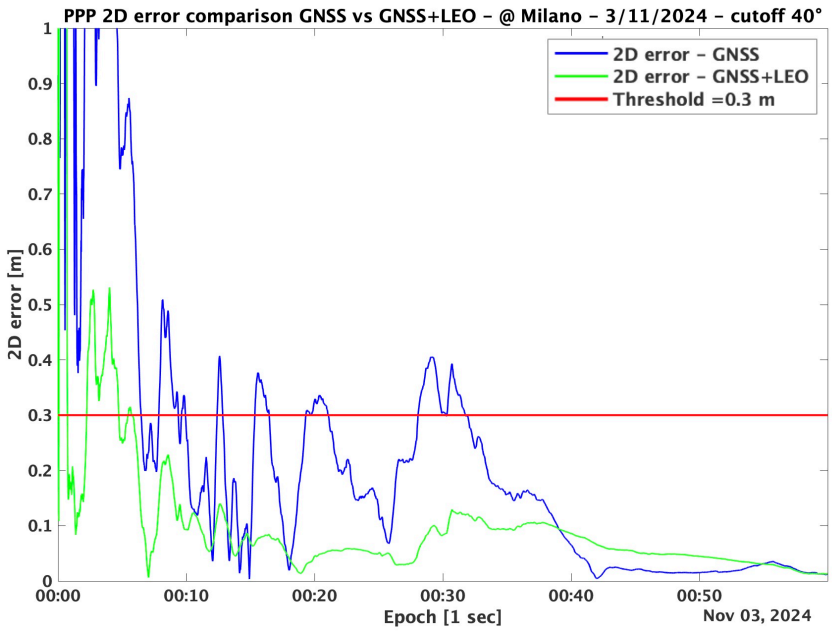

Figure 5: Comparison of 2D error over time for GNSS-only (bleìue) configuration and hybrid GNSS+LEO (green) configuration for Test 3 (DOY: 308)

Table 3
Statistical anlysis of hybrid GNSS+LEO results.

Test	**Mean** [m]			**STD** [m]		
	East	North	Up	East	North	Up
1	0.02	0.01	0.01	0.00	0.00	0.03
2	0.03	0.06	0.01	0.00	0.00	0.04
3	0.01	0.01	0.05	0.00	0.00	0.02

4. Conclusions

In this work, we developed a dedicated software for simulating LEO observations and processing GNSS+LEO measurements. The results demonstrate significant improvements in the convergence of the PPP solution, highlighting the advantages of integrating LEO satellites. The increased number of satellites in line-of-sight and their rapid motion contribute to a faster and more stable solution in harsh environments, simulated by applying 40-degree cutoff on satellites' elevation. Moreover, the statistical analysis confirms a reduction in positioning errors, particularly in the horizontal components. Future work will focus on testing the proposed approach in kinematic conditions and extending the simulation framework to include LEO phase observations. Additionally, a measurement campaign in an urban environment will be conducted to validate the methodology with real field data, further assessing the performance in dynamic and challenging scenarios.

Declaration on Generative AI

The authors have not employed any Generative AI tools.

References

[1] P. Teunissen, O. Montenbruck, Springer Handbook of Global Navigation Satellite Systems, 1st ed., Springer, 2017.

[2] A. Leick, L. Rapoport, D. Tatarnikov, GPS Satellite Surveying, 4th ed., Wiley, New York, NY, USA, 2015.

[3] J. Kouba, F. Lahaye, P. Tetreault, Precise point positioning, in: Springer Handbook of Global Navigation Satellite Systems, Springer, 2017, pp. 723–751.

[4] R. Dach, S. Lutz, P. Walser, P. Fridez, Bernese GNSS Software Version 5.2, Documentation, Astronomical Institute, Technical Report, University of Bern, 2015.

[5] D. Gebre-Egziabher, S. Gleason, GNSS Applications and Methods, Artech House, 2009.

[6] A. Leick, L. Rapoport, D. Tatarnikov, GPS Satellite Surveying, John Wiley & Sons, 2015.

[7] F. S. T. V. Diggelen, A-GPS: Assisted GPS, GNSS, and SBAS, Artech House, 2009.

[8] L. T. Hsu, S. S. Jan, P. D. Groves, et al., Multipath mitigation and nlos detection using vector tracking in urban environments, GPS Solutions 19 (2015) 249–262.

[9] N. Zhu, J. Marais, D. Bétaille, M. Berbineau, Gnss position integrity in urban environments: A review of literature, IEEE Transactions on Intelligent Transportation Systems 19 (2018) 2762–2778.

[10] T. Kos, I. Markezic, J. Pokrajcic, Effects of multipath reception on gps positioning performance, in: Proceedings ELMAR-2010, 2010, pp. 399–402.

[11] L. Meng, L. Yang, W. Yang, L. Zhang, A survey of gnss spoofing and anti-spoofing technology, Remote Sensing 14 (2022) 4826.

[12] A. Broumandan, R. Siddakatte, G. Lachapelle, An approach to detect gnss spoofing, IEEE Aerospace and Electronic Systems Magazine 32 (2017) 64–75.

[13] G. X. Gao, M. Sgammini, M. Lu, N. Kubo, Protecting gnss receivers from jamming and interference, Proceedings of the IEEE 104 (2016) 1327–1338.

[14] M. Alghisi, L. Biagi, Positioning with gnss and 5g: Analysis of geometric accuracy in urban scenarios, Sensors 23 (2023) 2181.

[15] C. Pileggi, F. C. Grec, L. Biagi, 5g positioning: An analysis of early datasets, Sensors 23 (2023) 9222.

[16] M. Brambilla, M. Alghisi, B. C. Tedeschini, A. Fumagalli, F. C. Grec, L. Italiano, C. Pileggi, L. Biagi, S. Bianchi, A. Gatti, A. Goia, M. Nicoli, E. Realini, Integration of 5g and gnss technologies for enhanced positioning: An experimental study, IEEE Open Journal of the Communications Society 5 (2024) 7197–7215.

[17] W. Li, Q. Yang, X. Du, et al., Leo augmented precise point positioning using real observations from two centispace™ experimental satellites, GPS Solutions 28 (2024) 44.

[18] G. Singh, Satellite communication constellations as sources of alternate pnt (position, navigation, and timing), in: IET Conference Proceedings, volume 2022, 2023, pp. 176–185.

[19] F. S. Prol, S. Kaasalainen, E. S. Lohan, M. Z. H. Bhuiyan, J. Praks, H. Kuusniemi, Simulations using leo-pnt systems: A brief survey, in: 2023 IEEE/ION Position, Location and Navigation Symposium (PLANS), 2023, pp. 381–387.

[20] L. Ries, M. C. Limon, F.-C. Grec, M. Anghileri, R. Prieto-Cerdeira, F. Abel, J. Miguez, J. V. Perello-Gisbert, S. D'Addio, R. Ioannidis, A. Ostillio, M. Rapisarda, R. Sarnadas, P. Testani, Leo-pnt for augmenting europe's space-based pnt capabilities, in: 2023 IEEE/ION Position, Location and Navigation Symposium (PLANS), 2023, pp. 329–337.

[21] M. Li, T. Xu, M. Guan, et al., Leo-constellation-augmented multi-gnss real-time ppp for rapid re-convergence in harsh environments, GPS Solutions 26 (2022) 29.

[22] L. Mottinelli, Exploring scientific opportunities with low earth orbit positioning, navigation, and timing (leo pnt): Potential applications in gnss, in: 9th International Colloquium on Scientific and Fundamental Aspects of GNSS, European Space Agency (ESA), Poland, 2024. Presented at the conference.

[23] R. O. Perez, M. C. Limon, P. Giordano, R. Prieto-Cerdeira, Mixing real and simulated observables to assess the performance of hybrid gnss/leo-pnt precise positioning, in: Proceedings of the 37th

International Technical Meeting of the Satellite Division of The Institute of Navigation (ION GNSS+ 2024), Baltimore, MD, USA, 2024, pp. 2308–2322.

[24] M. I. Ribeiro, Kalman and Extended Kalman Filters: Concept, Derivation and Properties, Technical Report, Institute for Systems and Robotics, 2004.